

AD-A277 451



(2)

Characteristics of Ion Flow in the Quiet State of the Inner Plasma Sheet

15 March 1994

Prepared by

V. ANGELOPOULOS, C. F. KENNEL, F. V. CORONITI, R. PELLAT,
M. G. KIVELSON, R. J. WALKER, and C. T. RUSSELL
UCLA

H. E. SPENCE
Space and Environment Technology Center
Technology Operations
The Aerospace Corporation

W. BAUMJOHANN
MPI für Extraterrestrische Physik

and

W. C. FELDMAN and J. T. GOSLING
Los Alamos National Laboratory

DTIC
ELECTE
MAR 28 1994
S F D

Prepared for

SPACE AND MISSILE SYSTEMS CENTER
AIR FORCE MATERIEL COMMAND
2430 E. El Segundo Boulevard
Los Angeles Air Force Base, CA 90245

Engineering and Technology Group

APPROVED FOR PUBLIC RELEASE;
DISTRIBUTION UNLIMITED

AEROSPACE
CORPORATION
California

DTIC PRESENTATION


94 3 25 073

94-09383

This report was submitted by The Aerospace Corporation, El Segundo, CA 90245-4691, under Contract No. F04701-88-C-0089 with the Space and Missile Systems Center, 2430 E. El Segundo Blvd., Suite 6037, Los Angeles AFB, CA 90245-4687. It was reviewed and approved for The Aerospace Corporation by A. B. Christensen, Principal Director, Space and Environment Technology Center. Capt. Leslie O. Belsma was the project officer for the Mission-Oriented Investigation and Experimentation (MOIE) program.

This report has been reviewed by the Public Affairs Office (PAS) and is releasable to the National Technical Information Service (NTIS). At NTIS, it will be available to the general public, including foreign nationals.

This technical report has been reviewed and is approved for publication. Publication of this report does not constitute Air Force approval of the report's findings or conclusions. It is published only for the exchange and stimulation of ideas.


Leslie O. Belsma, CAPT, USAF
MOIE Program Manager


WILLIAM KYLE SNEDDON, CAPT, USAF
Deputy Chief
Industrial and International Division

REPORT DOCUMENTATION PAGE			Form Approved OMB No. 0704-0188	
Public reporting burden for this collection of information is estimated to average 1 hour per response, including the time for reviewing instructions, searching existing data sources, gathering and maintaining the data needed, and completing and reviewing the collection of information. Send comments regarding this burden estimate or any other aspect of this collection of information, including suggestions for reducing this burden to Washington Headquarters Services, Directorate for Information Operations and Reports, 1215 Jefferson Davis Highway, Suite 1204, Arlington, VA 22202-4302, and to the Office of Management and Budget, Paperwork Reduction Project (0704-0188), Washington, DC 20503.				
1. AGENCY USE ONLY (Leave blank)		2. REPORT DATE 15 March 1994		3. REPORT TYPE AND DATES COVERED
4. TITLE AND SUBTITLE Characteristics of Ion Flow in the Quiet State of the Inner Plasma Sheet			5. FUNDING NUMBERS F04701-88-C-0089	
6. AUTHOR(S) Angelopoulos, V., Kennel, C. F., Coroniti, F. V., Pellat, R., Kivelson, M. G., Walker, R. J., and Russell, C.T. (UCLA); Spence, H.E. (The Aerospace Corporation); Baumjohann, W. (MPD); Feldman, W. C., and Gosling, J. T. (Los Alamos)				
7. PERFORMING ORGANIZATION NAME(S) AND ADDRESS(ES) The Aerospace Corporation Technology Operations El Segundo, CA 90245-4691			8. PERFORMING ORGANIZATION REPORT NUMBER TR-93(3940)-7	
9. SPONSORING/MONITORING AGENCY NAME(S) AND ADDRESS(ES) Space and Missile Systems Center Air Force Materiel Command 2430 E. El Segundo Blvd. Los Angeles Air Force Base, CA 90245			10. SPONSORING/MONITORING AGENCY REPORT NUMBER SMC-TR-94-04	
11. SUPPLEMENTARY NOTES				
12a. DISTRIBUTION/AVAILABILITY STATEMENT Approved for public release; distribution unlimited			12b. DISTRIBUTION CODE	
13. ABSTRACT (Maximum 200 words) We use AMPTE/IRM and ISEE 2 data to study the properties of the high beta ($\beta_t > 0.5$) plasma sheet, the inner plasma sheet (IPS). Bursty bulk flows (BBFs) are excised from the two databases, and the average flow pattern in the non-BBF (quiet) IPS is constructed. At local midnight this ensemble-average flow is predominantly duskward; closer to the flanks it is mostly earthward. The flow pattern agrees qualitatively with calculations based on the <i>Tsyganenko</i> [1987] model (T87), where the earthward flow is due to the ensemble-average cross tail electric field and the duskward flow is the diamagnetic drift due to an inward pressure gradient. The IPS is on the average in pressure equilibrium with the lobes. Because of its large variance the average flow does not represent the instantaneous flow field. Case studies also show that the non-BBF flow is highly irregular and inherently unsteady, a reason why earthward convection can avoid a pressure balance inconsistency with the lobes. The ensemble distribution of velocities is a fundamental observable of the quiet plasma sheet flow field.				
14. SUBJECT TERMS Convection Magnetosphere Plasma Sheet			15. NUMBER OF PAGES 9	
			16. PRICE CODE	
17. SECURITY CLASSIFICATION OF REPORT Unclassified	18. SECURITY CLASSIFICATION OF THIS PAGE Unclassified	19. SECURITY CLASSIFICATION OF ABSTRACT Unclassified	20. LIMITATION OF ABSTRACT	

CONTENTS

Abstract	2
Introduction	2
Ensemble-Average Properties of the Quiet IPS.....	2
On the Properties of Convection in the Quiet IPS.....	4
Conclusions.....	5
References.....	5

FIGURES

1. Ion flow averages in each $3 \times 3 R_E^2$ X-Y bin.....	3
2. Averages of $E_Y = V_X B_Z$ in $3 R_E$ bins across the tail, for all data tailward of $X_{AGSM} < -10 R_E$	3
3. Ion flows calculated from the T87 model with the electric field from Figure 2 and the average density in each $3 \times 3 R_E^2$ X-Y bin as input.....	4
4. Variation of the measured ion pressure, P_i , with downtail distance at local midnight and at other Y_{AGSM} locations; and P_i constancy across the tail, 16–19 R_E downtail	4
5. (a) Scatterplot of the ensemble of flows observed by ISEE 2 in a $3 \times 3 R_E^2$ bin; (b) hodogram of the flow during a continuous two hour, geomagnetically quiet interval that contributed to the scatterplot; (c) the cross-tail electric field $E_Y = V_X B_Z$ derived from the same time interval	4

CHARACTERISTICS OF ION FLOW IN THE QUIET STATE OF THE INNER PLASMA SHEET

V. Angelopoulos^{1,2}, C. F. Kennel^{1,2}, F. V. Coroniti¹, R. Pellat¹,
H. E. Spence³, M. G. Kivelson², R. J. Walker²,
W. Baumjohann⁴, W. C. Feldman⁵, J. T. Gosling⁵, C. T. Russell²

Abstract We use AMPTE/IRM and ISEE 2 data to study the properties of the high beta ($\beta_i > 0.5$) plasma sheet, the inner plasma sheet (IPS). Bursty bulk flows (BBFs) are excised from the two databases, and the average flow pattern in the non-BBF (quiet) IPS is constructed. At local midnight this ensemble-average flow is predominantly duskward; closer to the flanks it is mostly earthward. The flow pattern agrees qualitatively with calculations based on the *Izyanenko* [1987] model (T87), where the earthward flow is due to the ensemble-average cross tail electric field and the duskward flow is the diamagnetic drift due to an inward pressure gradient. The IPS is on the average in pressure equilibrium with the lobes. Because of its large variance the average flow does not represent the instantaneous flow field. Case studies also show that the non-BBF flow is highly irregular and inherently unsteady, a reason why earthward convection can avoid a pressure balance inconsistency with the lobes. The ensemble distribution of velocities is a fundamental observable of the quiet plasma sheet flow field.

Introduction

The average flow velocity in the central plasma sheet is small (~ 50 km/s) due to the predominance of low velocity flows [Huang and Frank, 1986; Baumjohann et al., 1989]. However, although the central plasma sheet ion flow is most often nearly stagnant and with no preferred direction, it is interrupted by high speed (> 400 km/s) earthward flow bursts [Baumjohann et al., 1989]. The flow bursts are more frequent during geomagnetically disturbed times (resulting in a positive correlation of the average flow velocity with AE) but may take place even during low AE conditions.

The plasma and magnetic field variations concurrent with the bursts of flow in the inner central plasma sheet (ICPS) (i.e., where $B_{XY} = (B_X^2 + B_Y^2)^{1/2} < 15$ nT, or $B_Z/B_{XY} > 0.5$) were studied by Angelopoulos et al. [1992]. They argued that flow bursts have a time-scale of the order of 1 min, they correlate with dipolarization and heating of the plasma sheet, and are embedded in flow enhancement intervals of the order of 10 min, termed bursty bulk flow events (BBFs). BBFs reside, at least partially, close to the neutral sheet; thus they represent local plasma acceleration. Since the plasma sheet can be active even during low AE, categorization of the plasma sheet states based on BBFs and irrespective of geomagnetic activity may be a fruitful way of organizing plasma sheet studies. We adopt this approach in our paper.

Ensemble-Average Properties of the Quiet IPS

We used plasma moments from the 3D plasma instrument and magnetic field data from the fluxgate magnetometer on AMPTE/IRM from the 1985 magnetotail crossings (01/23/85 – 06/31/85) at 5 s resolution. We also used plasma moments from the Los Alamos/MPI Fast Plasma Experiment (FPE) and magnetic field data from the UCLA fluxgate magnetometer on ISEE 2 from the 1978 and 1979 magnetotail crossings (12/26/77 – 06/30/78 and 12/31/78 – 06/06/79). The FPE plasma data were calculated at 3 s or 12 s resolution depending on the orbit. They were block averaged with a 12 s window and were merged with magnetic field data of the same resolution. The ISEE 2 orbit extended our analysis beyond the apogee of IRM (19 R_E), out to 22 R_E and complemented IRM's limited coverage in the post-midnight sector.

We transformed the satellite position in an Aberrated Geocentric Solar Magnetospheric (AGSM) system using a 4.5° aberration angle. We limited our databases to $X_{AGSM} < -7 R_E$, since earthward of that the particle detectors may miss a considerable part of the ion distribution, and within $|Y_{AGSM}| < 15 R_E$ to avoid magnetopause crossings. Lobe intervals were removed by requiring that the ion energy density E_i be above noise level ($E_i > 0.01$ ergs/cm³). In addition, we identified potential remaining magnetopause boundary crossings by searching for times when the ion temperature T_i dropped below 500 eV, the ion density N_i increased beyond 1 cm⁻³ and the flow was persistently (> 5 min) tailward (> 200 km/s) at distances of $|Y| > 10 R_E$. These were removed based on the times of the rotation of the field from the magnetospheric to the magnetosheath direction. Mantle crossings were also removed from the region $\sqrt{Y_{AGSM}^2 + Z_{AGSM}^2} > 10 R_E$ and $Z_{AGSM} > 6 R_E$ based on the same criteria as the potential magnetopause crossings.

We identified two plasma sheet regimes that display rather consistent field elevations (i.e., the angle between **B** and the X-Y plane). These are: a high beta region ($\beta_i > 0.5$) that incorporates the high elevation ICPS and is closest to the neutral sheet, and a low beta region of lobe-like elevation, that includes the PSBL, as defined by Baumjohann et al., [1989]. We termed the two regions inner and outer plasma sheet respectively (IPS, OPS) to distinguish them from regions previously identified by other criteria.

We defined BBFs to be plasma sheet segments of continuous ion flow magnitude $V_i > 100$ km/s, during which V_i exceeds 400 km/s at least once in the IPS. Flows above 400 km/s that were separated by less than 10 min were considered parts of the same BBF event. The IRM (ISEE 2) dataset contained 100 (200) events. The median BBF duration was ~ 550 s in both datasets. We excised the BBFs and further restricted our database to the IPS by eliminating samples with $\beta_i < 0.5$. The final non-BBF, IPS dataset represents 92% (94%) of the total IPS dataset of IRM (ISEE 2) and is composed of 167,619 (173,417) samples.

Figure 1 shows average velocities derived from one or more hours of data in each $3 \times 3 R_E^2$ bin projected on the X-Y plane. Velocities are in GSM coordinates for IRM and in spacecraft coordinates (very close to GSE) for ISEE 2. The flow averages are small compared to the lowest energy measurable by the 3D and FPE instruments (equivalent to

¹Dept. of Physics, UCLA, Los Angeles, CA

²IGPP, UCLA, Los Angeles, CA

³The Aerospace Corporation, Los Angeles, CA

⁴MPI für extraterrestrische Physik, Garching, Germany

⁵Los Alamos National Laboratory, Los Alamos, NM

Codes	
Dist	Ave. dist for Special
A-1	

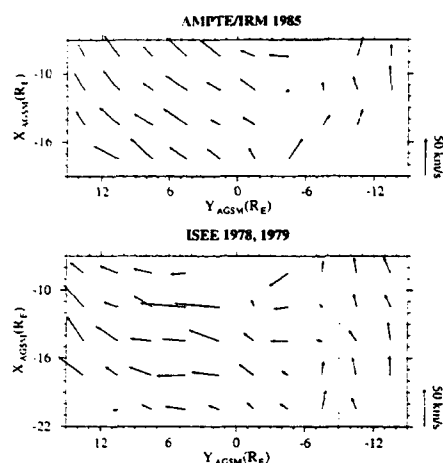


Fig. 1. Ion flow averages in each $3 \times 3 R_E^2$ X-Y bin.

53 km/s and 120 km/s respectively), but still within the velocity resolution of the instruments. The consistency of the statistically independent flow averages in each dataset, as well as the rough correspondence between results from the two different instruments indicate that the averages are meaningful. The ion flow near the midnight and pre-midnight sectors has a significant duskward component. At around local midnight the duskward flow component is comparable to, or larger than the earthward component. The earthward component becomes dominant closer to the flanks.

In the two-fluid approximation, two components contribute to the ion velocity \mathbf{V} : a drift due to an electric field \mathbf{E} , and a diamagnetic drift \mathbf{V}_D consistent with the plasma pressure profile, i.e., $\mathbf{V} = \mathbf{V}_E \times \mathbf{B} + \mathbf{V}_D$ [Chen, 1974]. In the plasma sheet, ions and electrons drift diamagnetically in opposite directions with speeds proportional to their respective pressure gradients, and create a diamagnetic current consistent with the overall current profile in the plasma sheet. The electron temperature is small relative to the ion temperature by a fairly constant factor of 7–8 (e.g., Baumjohann et al. [1989]). Assuming the same relationship for the ratio of the pressure gradients, we neglect the electron contribution to the diamagnetic current. We thus estimate the magnitude of the diamagnetic drift from the cross-tail current $\mathbf{J} = \nabla \times \mathbf{B} / \mu_0$ according to: $\mathbf{V}_D = \nabla \times \mathbf{B} / (\mu_0 N_i q_e)$, where N_i is the ion density, q_e is the electron charge and μ_0 is the magnetic permeability of free space. For a current sheet thickness equal to a plasma sheet half thickness at local midnight of $3 R_E$, a tail-lobe field of 30 nT, and an ion density of 0.3 cm^{-3} we get $V_D \approx 25 \text{ km/s}$. This is comparable to the magnitude of the duskward components of the average flow vectors at local midnight in Figure 1.

Assuming that tailward of $X = -10 R_E$ the diamagnetic drift is the dominant contribution to the average cross-tail flow and corotation is negligible, we decomposed the IPS velocity into an earthward $\mathbf{E} \times \mathbf{B}$ flow, and a duskward diamagnetic drift. To estimate the electric field associated with the earthward flow component in that region we computed the average of $E_Y = \mathbf{V} \times \mathbf{B}_Z$ in $3 R_E$ Y-bins. The result is presented in Figure 2. IRM (ISEE 2) data are shown in GSM (spacecraft) coordinates.

The average cross-tail electric field is small (0.4–0.5 kV/ R_E) and non-uniform across the tail: it is depressed at local midnight and maximizes closer to the tail boundary. An enhancement of the average E_Y at $-3 < Y_{AGSM} < 6 R_E$ in both datasets may be due to incomplete removal of BBF-induced flow in that region, possibly indirectly related to nearby BBFs (the BBF occurrence rate, not shown here, peaks

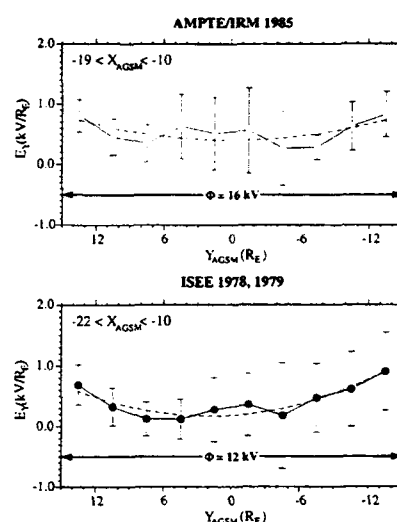


Fig. 2. Averages of $E_Y = \mathbf{V} \times \mathbf{B}_Z$ in $3 R_E$ bins across the tail, for all data tailward of $X_{AGSM} < -10 R_E$. Error bars are a fifth of the standard deviation about the mean. The dashed line is a second order polynomial fit to the averages. Φ is the average potential drop across the sampled region.

at local midnight). Error bars represent a fifth of the standard deviation about the mean suggesting that the fluctuations of E_Y are much larger than the average. However, the consistency of the average cross-tail E_Y pattern between the two datasets implies that the averages are probably significant. The total potential drop Φ across the $30 R_E$ section of the magnetotail studied here is 16 kV and 12 kV for the two datasets respectively, consistent with the "resting" 7–38 kV potential drop across the polar cap [Reiff and Luhmann, 1986]. The magnitude and the shape of the electric field give us confidence that we have properly removed from our datasets convection that is directly related to reconnection. We use a second order polynomial fit to model the Y-dependence of E_Y . We get the expressions: $E_Y = 0.39 + 0.41 (Y/15)^2$ and $E_Y = 0.17 - 0.18 (Y/15) + 0.70 (Y/15)^2$, for the IRM and ISEE 2 datasets respectively, where E_Y is in kV/ R_E and Y is in R_E .

We can use an empirical magnetic field model of the magnetotail to calculate the expected velocity vectors in the quiet IPS, assuming that the above polynomial fit of E_Y can be applied also earthward of $|X| = 10 R_E$, including corotation, and using the average ion density in each $3 \times 3 R_E$ X-Y bin as input to the calculation of \mathbf{V}_D . We used the short version of the Tsyganenko [1987] (T87) model for $K_p = 0$ to compute the magnetic field and its spatial derivatives. Since the current density and, thus, the diamagnetic drift depend on the distance away from the equatorial plane we computed the average drift over Z-distances for which J/J_{eq} remained above J_{min}/J_{eq} , where J_{eq} is the maximum, equatorial current density in the T87 model. The choice of J_{min}/J_{eq} is somewhat arbitrary; we set $J_{min}/J_{eq} = 0.9$ because the model drifts were small when integrated over a wider current sheet region. Since the T87 model tends to overestimate the current sheet thickness [Fairfield, 1991], and thus underestimate the equatorial current sheet density, our choice of a fairly narrow integration region may be reasonable. Our results are projected on the equatorial plane in Figure 3. There is qualitative agreement between the model calculations and the average velocities of Figure 1; in particular, the model reproduces the predominantly duskward flows near local midnight and the predominantly earthward flows closer to the magnetotail boundaries.

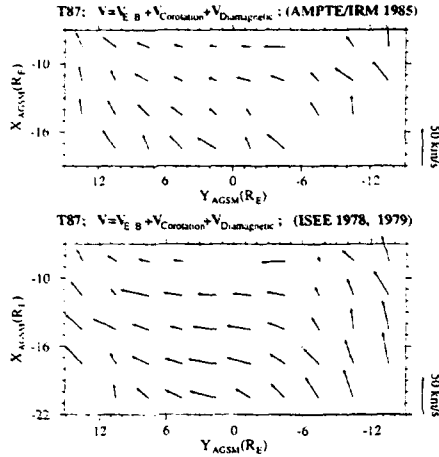


Fig. 3. Ion flows calculated from the T87 model with the electric field from Figure 2 and the average density in each $3 \times 3 R_E^2$ X-Y bin as input.

On the Properties of Convection in the Quiet IPS

Erickson and Wolf [1980] argued that a "pressure balance inconsistency" arises for laminar, steady, sunward convection in a realistic tail configuration. The pressure of an adiabatically convected flux tube from the distant tail to the near earth regions increases too rapidly to be consistent with lobe pressure observations. Tsyganenko [1982] suggested that cross tail drifts could remove part of the pressure of an earthward convecting flux tube. Kivelson and Spence [1988] showed

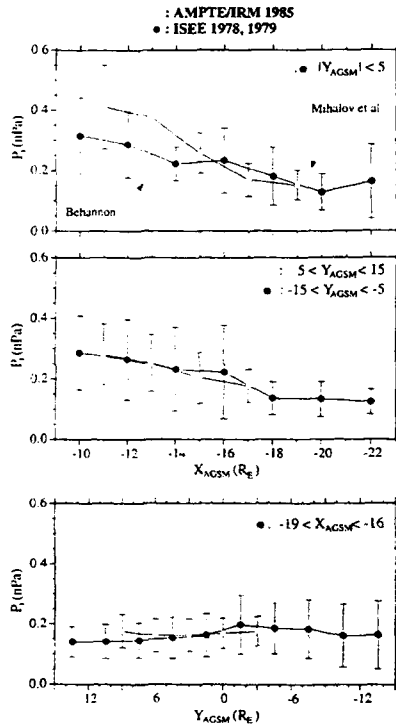


Fig. 4. Variation of the measured ion pressure, P_i , with down-tail distance at local midnight (top panel) and at other Y_{AGSM} locations (middle panel). Bottom panel: P_i constancy across the tail, 16–19 R_E downtail.

that equatorial ∇B drifts are sufficient to accomplish this task at the midnight meridian, given a finite tail-width. However, the ∇B drift changes sign away from the equatorial plane and the equatorial magnetization drift can be much larger in sign and opposite from the ∇B drift in a tail configuration (Bird and Beard [1972], see their Figure 7). Although the bounce averaged sum of the particle gradient, curvature and magnetization drifts has not yet been considered, the sum of the above drifts integrated over an isotropic maxwellian distribution is equivalent to the diamagnetic drift that appears in the fluid equations of motion (e.g., see Bird and Beard [1972], Eq. 4) and was used in the previous section. In accordance with the suggestion of Tsyganenko [1982], the cross tail drifts in the midnight sector are equal to or larger than the earthward, convective velocity and therefore the proposed pressure balance inconsistency argument may not apply. It may, however, apply away from midnight, where the flow is predominantly earthward. We thus first investigated how the IPS ion pressure P_i changes across the magnetotail as well as with distance from Earth. Figure 4 presents the results of this investigation.

The bottom panel shows averages of P_i between 16 and 19 R_E downtail, calculated by using a $7 R_E$ sliding window in the Y_{AGSM} direction on $3 R_E$ centers. To reduce the large scatter due to the variability of the solar wind dynamic pressure we only accepted averages constructed from more than 7 hours of data. P_i is fairly constant across the tail. The near-quantitative agreement between the average pressure values from the two instruments is additional confirmation that the trends are meaningful. The top two panels show the variation of the average ion pressure with down-

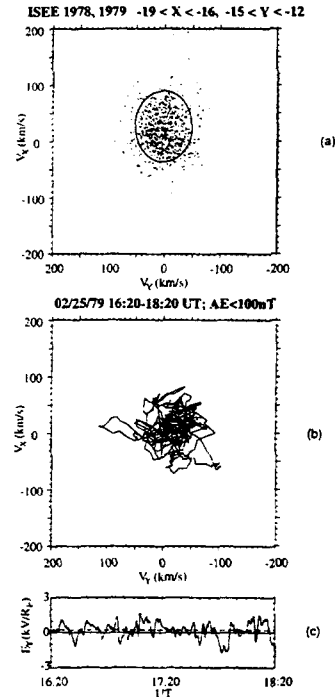


Fig. 5. (a) Scatterplot of the ensemble of flows observed by ISEE 2 in a $3 \times 3 R_E^2$ bin. The average vector and the ellipse representing the standard deviation of the velocity along the principal axes directions (which are essentially earthward and duskward for this bin) are also shown. (b) Hodogram of the flow (running-averaged at 1 min) during a continuous two hour, geomagnetically quiet interval that contributed to the scatterplot. (c) The cross-tail electric field $E_y = V_x B_z$ derived from the same time interval (the dashed line is the average).

tail distance. The averages of P_i were calculated using a $2 \times 10 R_E$ bin in the X-Y direction. Both in the midnight meridian (as previously noted by Spence *et al.* [1989]) and closer to the magnetotail boundary, the pressure decreases slowly with decreasing X. The observed P_i averages agree to within a standard deviation with the magnetic pressure determined from the fits to the observed values of the lobe field magnitude B_L and their dependence on radial distance R, reported by Mihalov *et al.* [1968] ($B_L = 191.4 \cdot R^{-0.736}$) and on downtail GSE distance reported by Behannon [1968] ($B_L = -10.72 + 69.13 \cdot X_{GSE}^{-0.3} + 1.3 \cdot K_P + 0.07 \cdot Z_{SM}$; Z_{SM} is the distance from the solar magnetospheric equator). The lobe pressure curves are plotted on panels 5(a) and 5(b) after substituting X_{AGSM} for R in the fit of Mihalov *et al.* [1968] and assuming $X_{GSE} \approx X_{AGSM}$, $K_P = 0$ and $Z_{SM} = 0$ in the fit of Behannon [1968]. Thus, plasma sheet convection avoids a pressure balance inconsistency even away from midnight, where the flow is mostly earthward. In the following, we argue that this happens because non-BBF convection violates one of the basic assumptions of the pressure balance inconsistency argument, namely that the flow is steady.

The Instantaneous Flow Pattern

Although the ensemble average velocities and electric fields point towards a quasi-steady magnetospheric configuration, the standard deviation about their mean paints a rather different picture. Figure 5(a) shows a scatterplot of the ISEE 2 flow samples used to construct an average vector in the morning sector. It is evident that the scatter of the data is much larger than the average itself. Figure 5(b) shows a hodogram of the flow vector for a 2 hour interval of low AE conditions selected from the same bin; the large variability of the flow is not only a property of the statistical ensemble but of the time series of the plasma flow as well. Figure 5(c) shows the inferred electric field during this interval. E_y is variable; its range of variation is much larger than its average.

Figure 5 suggests that the non-BBF plasma sheet flow, and the convection electric field associated with it, exhibit large variability even during geomagnetically quiet times. The slow sunward convection is thus the average of relatively large velocity variations inherent to the plasma sheet flow. The flow pattern of Figure 1 is not representative of the instantaneous flow streamlines since at any given time the flow can point towards any X-Y direction and its magnitude can be several times larger than its time-average. A small dawn-dusk electric field emerges only after averaging the instantaneous electric field that can point downward almost as often as duskward with an oscillation peak-to-peak amplitude that can be an order of magnitude larger than its average.

Conclusions

We reproduced the average flow pattern of the quiet IPS assuming that the flow is the sum of corotation, an $E \times B$ flow and a diamagnetic drift consistent with the T87 model. The above simple scheme explains qualitatively the basic features of the ensemble-average ion flow pattern in the plasma sheet based on what must be considered an ensemble-average magnetic field. However, both in the ensemble distributions as well as at any given time the flow variance is several times larger than the average flow itself. The inferred electric field exhibits a similar variability. The instantaneous flow field does not agree with the average flow pattern, but may point in any direction at any given X-Y location. Thus, the quiet IPS flow is not steady. The average flow pattern is a by-product of a more complicated system whose fundamental observable is the ensemble distribution of velocities. The flow variability may enable the IPS pressure to adjust to the lobe pressure, and allow slow, earthward convection to proceed in an average sense. The properties of this variability (amplitude, direction, spatial dependence) can be central in

understanding the physical mechanisms that couple the quiet IPS with the drivers of earthward convection.

Acknowledgments. It has become known to us during this work that X. Zhu also looked at the average flow pattern in the plasma sheet and has independently reached similar observational conclusions. We would like to thank C. M. Hammond for his help with the aberration of the position data. V.A. and C.F.K. were supported by grants NSF ATM 91-20591 and LANL/UCRP 304. F.V.C. and R.P. were supported by NASA grant NAGW 2620. H.E.S. was supported by the Air Force Materiel Command's Space and Missile Systems Center under contract F04701-88-C-0089. M.G.K. was supported by NSF grant ATM 91-15557. R.J.W. was supported by NASA grant NAG5-1530. C.T.R. was supported by NASA grant NAG5-1967.

References

- Angelopoulos, V., *et al.*, Bursty bulk flows in the inner central plasma sheet, *J. Geophys. Res.*, 97, 4027, 1992.
- Baumjohann, W., *et al.*, Average plasma properties in the central plasma sheet, *J. Geophys. Res.*, 94, 6597, 1989.
- Behannon, K. W., Mapping of the Earth's bow shock and magnetic tail by Explorer 33, *J. Geophys. Res.*, 73, 907, 1968.
- Bird, M. K., and D. B. Beard, The self-consistent geomagnetic tail under static conditions, *Planet. Space Sci.*, 20, 2057, 1972.
- Chen, F. F., *Introduction to Plasma Physics and Controlled Fusion*, 69 pp., Plenum Press, New York, 1984.
- Erickson, G. M., and R. A. Wolf, Is steady state convection possible in the earth's magnetosphere?, *Geophys. Res. Lett.*, 6, 897, 1980.
- Fairfield, D. H., An evaluation of the Tsyganenko magnetic field model, *J. Geophys. Res.*, 96, 1481, 1991.
- Huang, C. Y., and L. A. Frank, A statistical study of the central plasma sheet: Implications for substorm models, *Geophys. Res. Lett.*, 13, 652, 1986.
- Kivelson, M. G., and H. E. Spence, On the possibility of quasi-static convection in the quiet magnetotail, *Geophys. Res. Lett.*, 15, 1541, 1988.
- Mihalov, J. D., *et al.*, Configuration and reconnection of the geomagnetic tail, *J. Geophys. Res.*, 73, 6837, 1968.
- Reiff, P. H., and J. G. Luhmann, Solar wind control of the polar-cap voltage, in *Solar Wind-Magnetosphere Coupling*, edited by Y. Kamide and J. A. Slavin, p. 453, Terra Scientifica, Tokyo, 1986.
- Spence, H. E., *et al.*, Magnetospheric plasma pressures in the midnight meridian: Observations from 2.5 to 35 R_E , *J. Geophys. Res.*, 94, 5264, 1989.
- Tsyganenko, N. A., On the convective mechanism for formation of the plasma sheet in the magnetospheric tail, *Planet. Space Sci.*, 30, 1007, 1982.
- Tsyganenko, N. A., Global quantitative models of the geomagnetic tail in the cislunar magnetosphere for different disturbance levels, *Planet. Space Sci.*, 35, 1347, 1987.
- V. Angelopoulos, F. V. Coroniti, C. F. Kennel and R. Pellat, Dept. of Physics, UCLA, Los Angeles, CA 90024-1547.
- H. E. Spence, Space and Environmental Technology Center, The Aerospace Corporation, P.O. Box 92957, Los Angeles, CA 90009.
- M. G. Kivelson, C. T. Russell and R. J. Walker, Institute of Geophysics and Planetary Physics, UCLA, Los Angeles, CA 90024-1567.
- W. Baumjohann, Max-Planck-Institut für extraterrestrische Physik, D-8046, Garching, Germany.
- W. C. Feldman and J. T. Gosling, Los Alamos National Laboratory, SST-7, MS D-466, Los Alamos, NM 87545.

TECHNOLOGY OPERATIONS

The Aerospace Corporation functions as an "architect-engineer" for national security programs, specializing in advanced military space systems. The Corporation's Technology Operations supports the effective and timely development and operation of national security systems through scientific research and the application of advanced technology. Vital to the success of the Corporation is the technical staff's wide-ranging expertise and its ability to stay abreast of new technological developments and program support issues associated with rapidly evolving space systems. Contributing capabilities are provided by these individual Technology Centers:

Electronics Technology Center: Microelectronics, solid-state device physics, VLSI reliability, compound semiconductors, radiation hardening, data storage technologies, infrared detector devices and testing; electro-optics, quantum electronics, solid-state lasers, optical propagation and communications; cw and pulsed chemical laser development, optical resonators, beam control, atmospheric propagation, and laser effects and countermeasures; atomic frequency standards, applied laser spectroscopy, laser chemistry, laser optoelectronics, phase conjugation and coherent imaging, solar cell physics, battery electrochemistry, battery testing and evaluation.

Mechanics and Materials Technology Center: Evaluation and characterization of new materials: metals, alloys, ceramics, polymers and their composites, and new forms of carbon; development and analysis of thin films and deposition techniques; nondestructive evaluation, component failure analysis and reliability; fracture mechanics and stress corrosion; development and evaluation of hardened components; analysis and evaluation of materials at cryogenic and elevated temperatures; launch vehicle and reentry fluid mechanics, heat transfer and flight dynamics; chemical and electric propulsion; spacecraft structural mechanics, spacecraft survivability and vulnerability assessment; contamination, thermal and structural control; high temperature thermomechanics, gas kinetics and radiation; lubrication and surface phenomena.

Space and Environment Technology Center: Magnetospheric, auroral and cosmic ray physics, wave-particle interactions, magnetospheric plasma waves; atmospheric and ionospheric physics, density and composition of the upper atmosphere, remote sensing using atmospheric radiation; solar physics, infrared astronomy, infrared signature analysis; effects of solar activity, magnetic storms and nuclear explosions on the earth's atmosphere, ionosphere and magnetosphere; effects of electromagnetic and particulate radiations on space systems; space instrumentation; propellant chemistry, chemical dynamics, environmental chemistry, trace detection; atmospheric chemical reactions, atmospheric optics, light scattering, state-specific chemical reactions and radiative signatures of missile plumes, and sensor out-of-field-of-view rejection.